

## Leveraging Physical and Virtual On-Aircraft Sensors to Inform Maintenance Practices

Rebecca Skelton Marshall  
Luna Labs USA, LLC  
706 Forest St. #A  
Charlottesville, VA 22903

Floyd Steele  
Luna Labs USA, LLC  
706 Forest St. #A  
Charlottesville, VA 22903

Sam Kunselman  
QTEC Aerospace  
4955 Corporate Dr NW #300,  
Huntsville, AL 35805

Dan Christy  
Luna Labs USA, LLC  
706 Forest St. #A  
Charlottesville, VA 22903

Fritz Friedersdorf  
Luna Labs USA, LLC  
706 Forest St. #A  
Charlottesville, VA 22903

Matt Watson  
QTEC Aerospace  
4955 Corporate Dr NW #300,  
Huntsville, AL 35805

Rena Fish  
QTEC Aerospace  
4955 Corporate Dr NW #300,  
Huntsville, AL 35805

### ABSTRACT

Time-based inspection and maintenance intervals are a conventional method of corrosion monitoring on aircraft. However, as corrosion processes do not necessarily occur in scheduled events, these conventional maintenance practices can lead to over- or under-estimation of costly inspections. A shift toward evidence-based and data driven predictive maintenance using a combination of on-asset monitoring devices and component-level models could improve efficiency and reduce total ownership costs. In particular, a “virtual sensor”, *i.e.*, a trained model to predict the corrosion at a given location on the aircraft, can be leveraged to optimize the placement of physical real-time monitoring devices. This digital twin process can be applied to determine the corrosion susceptibility of a single aircraft, or to conduct a fleet-wide analysis. In this work, sensing device measurements deployed at varying locations will be used to demonstrate the applicability of severity tracking, through data-driven machine learning models. In particular, models will be trained on environmental parameters and leveraged to predict current (corrosion rate).

Key words: Galvanic corrosion, corrosion sensor, machine learning, CBM+, aircraft maintenance,

### INTRODUCTION

Material damage and loss can occur on metallic structures during ambient outdoor conditions through atmospheric corrosion, leading to high costs of maintenance and repair<sup>1</sup>. The severity of corrosion is dependent on the material(s), the geometry, and the environment. In particular, it is of interest to understand and classify environments based on their corrosivity for a given material configuration to inform and enhance maintenance practices<sup>2</sup>. That is, having scheduled maintenance based on usage and estimated severity, in contrast to generalized maintenance and inspection intervals applied across all scenarios. The former could save time, money, and resources by preventing excessive maintenance when it is not needed, such as in mild environments with low corrosive materials.

To investigate and quantify the impact of the environment on corrosion severity, many researchers have deployed experimental mass loss coupons to various locations<sup>3-6</sup>. Due to the discrete data pulls required for mass loss analysis, annual averages are often aggregated to determine severity. In particular, this process has been leveraged to create international standards and government reports<sup>5,7-9</sup>. Although these experiments have added tremendous value to the community through determining a relative environmental severity for a given location there exist inherent limitations of being costly from numerous required samples and analysis manhours, slow to receive meaningful data, and requiring a deployment footprint at the location of interest. In addition, basing corrosion predictions on annual averages of environment and corrosion severity parameters may miss important seasonal events and diurnal cycles which are known to have an impact on corrosion rates<sup>10</sup>. Recent advances with real-time monitoring device measurements overcome the sparse mass-loss datasets and need for annual averaging, but still require physical deployments at locations of interest<sup>11</sup>.

Therefore, there exist a need for model which can be trained on existing experimental deployments of coupons but can extrapolate the respective corrosion severity to additional locations without any of the three limitations described above. Finite element method (FEM) models have become popular to estimate corrosion severity, due to their fine spatial resolution and customizable geometries<sup>12-15</sup>. However, FEM models can be computationally expensive and are built on fundamental physical equations, requiring some knowledge of the underlying physical processes and mechanisms. Conversely, machine learning (ML) models are data-driven and non-physics based, allowing rapid first approximations of systems prior to the mechanistic knowledge and deeper FEM analysis<sup>10,16</sup>.

Such data-driven modeling efforts can be difficult, due to the large factorial of possible influencing features<sup>10</sup>. In particular, in the context of atmospheric corrosion, there has been such debate around which environmental features to investigate, with focus on ozone<sup>3,17,18</sup>, UV<sup>4,18,19</sup>, contaminants/pollutants<sup>4,6,20,21</sup>, wind/wave<sup>4,18,21</sup>, relative humidity (RH)<sup>18-22</sup> and temperature<sup>18,19,21,22</sup>, to name a few. In general, it is agreed upon that there are two main influencing factors of a given location on the corrosion severity: the saltiness and the wetness. Without either of these factors, a conducting electrolyte would not be feasible and atmospheric corrosion could not occur.

As there has been no consensus on which environmental parameters may be most influential towards the saltiness and wetness of a location, and therefore, the corrosion severity, prior ML modeling efforts have been developed and applied with varying feature input parameters. Although including every environmental feature may result in a comprehensive and robust model, many of the parameters have sparse records and may not be necessary to capture the relationship of the corrosion severity. Prior atmospheric corrosion ML modeling reported in literature has either included a multitude of environmental parameters as-available<sup>18,23,24</sup>, or has focused on a select few parameters<sup>25,26</sup>. There has yet to be a systematic study of a limited set of parameters to gauge their direct influence on predicting the corrosion severity.

Therefore, the focus of this work will attempt to begin this systematic study, through the development and analysis of multiple models with varying feature input parameters. In particular, the input features will range from broad to local environments, with the goal of predicting the corrosion severity to help inform and enhance maintenance practices.

## EXPERIMENTAL PROCEDURE

## Real-Time Sensor Measurements in Monitoring Device

Real-time corrosion and environment monitoring devices were leveraged in this work. These devices consisted of interdigitated electrodes (IDE) for measuring galvanic corrosion, single-alloy free corrosion, and solution conductance along with relative humidity (RH) and temperature sensors (Figure 1).

The IDE solution conductance sensor is comprised of two gold electrodes on an inert alumina substrate. The solution conductance over the IDE was determined via an electrochemical impedance measurement made between the two electrodes at 25 kHz with an applied peak-to-peak voltage signal of 20 mV. The measurement span of the solution conductance sensor was between 5  $\mu\text{S}$  and 10,000  $\mu\text{S}$ . The RH sensor has a range of 0% to 100% RH with an accuracy of  $\pm 2\%$  RH. The temperature sensor has an accuracy of  $\pm 0.2$   $^{\circ}\text{C}$  within the relevant temperature range.

The free corrosion IDE sensor consisted of AA7075-T6, while the galvanic corrosion IDE sensor consisted of AA7075-T6 coupled with A286. The former will be the focus of the investigation in this work, with an electrochemical impedance spectroscopy (EIS) based measurement leveraged to elicit a proxy of self-corrosion of the single material. Specifically, a cyclic potential of frequency 0.5 Hz and amplitude 10 mV was applied to the AA7075-T6 IDE, which were separated by an insulating material. The current reported is the RMS current measured in response to the applied signal, which is assumed to be proportional to the self-corrosion rate. The measurement span of the single-alloy corrosion sensor is between 0.005  $\mu\text{A}$  and 100  $\mu\text{A}$ .

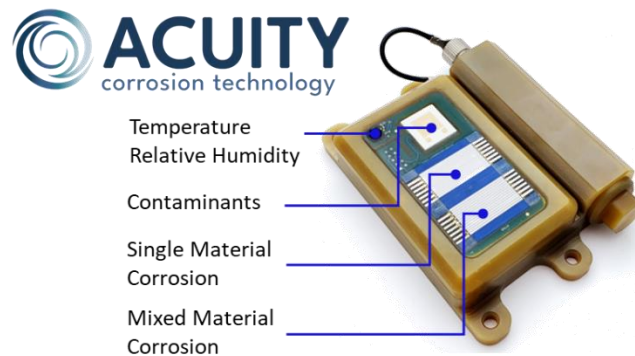


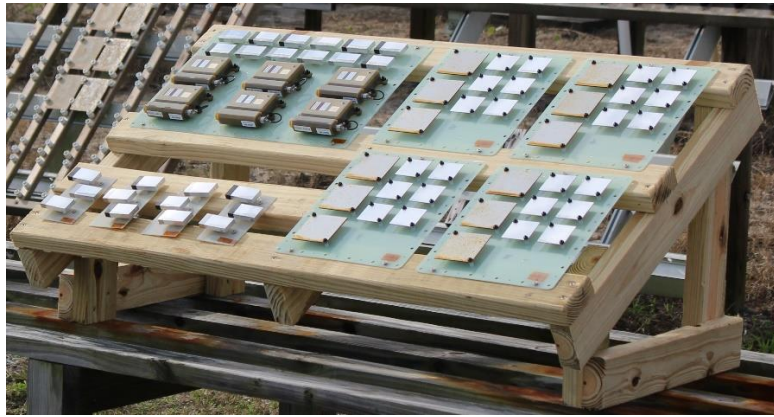
**Figure 1: Acuity LS sensing device for real-time environment and corrosion measurements<sup>1</sup>**

## Physical Device Deployment

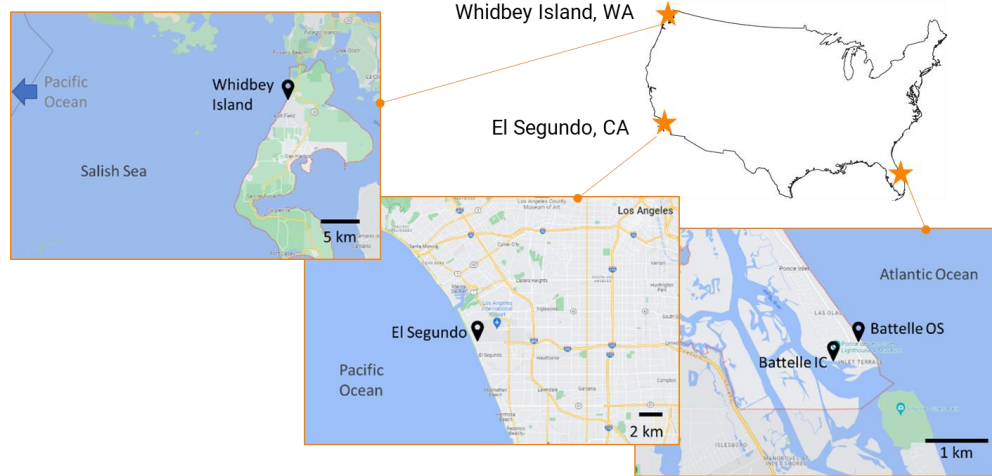
Monitoring devices and 1008 carbon steel witness coupons were deployed at four locations, mounted to a rack 5 feet off of the ground facing the main body of water with a 30° tilt from the horizontal (Figure 2). Whidbey Island, WA, El Segundo, CA, and Daytona Beach, FL all represented aggressive coastal environments at unique locations. Within Daytona Beach, FL an oceanside (OS) and 0.5 mi (800 m) intracoastal (IC) site were both considered, to determine the impact of the distance from the seacoast. Note that both Daytona Beach deployment sites were hosted on Battelle's Florida Materials Research Facilities (FMRF). Triplicate monitoring devices and triplicate mass loss witness coupons were exposed for a year, with the latter triplicates being pulled quarterly (3, 6, 9 12 month) (Table 1). After the respective exposure times, data was downloaded from the monitoring devices and the carbon steel coupons were grit blasted and weighted to determine the mass loss.

---

<sup>1</sup> Acuity LS, <https://acuitycorrosion.com/>



(a)



(b)

**Figure 2: (a) Example outdoor deployment rack and (b) map of four outdoor deployment locations**

## Acquirement of Environmental Data

### NOAA Weather Stations

Hourly data over the entire year of 2021 was pulled from NOAA weather stations located in three distinct locations of interest: Daytona Beach, Florida; El Segundo, California; Whidbey Island, Washington (Table 1). Note that one weather station was used to represent both Daytona Beach IC and OS, due to the spatial resolution of available weather stations. Air temperature (T) and dew point were then used to directly calculate the hourly-resolved relative humidity (RH) at each location.

Wind speed and wind direction were used to calculate a total *effective* wind that may contribute to salt deposition on-shore. In particular, it was assumed that wind directed orthogonal to the coastline would be most relevant to on-shore salt deposition when samples are positioned facing the ocean. Therefore, the resulting vector of total effective wind was determined at each location by accounting for the orientation of the coastline. It was assumed that wind speeds less than 4 m/s (9 mph) were not strong enough for salt deposition, and were therefore not included in the analysis.

### NOAA Buoy

Data was also pulled from off-shore buoy stations at half-hour resolution for the year of 2021. Wave height is known to contribute to salt deposition, in combination with the wind speed and direction<sup>21</sup>.

Therefore, wave heights greater than 0.5 m (1.6 ft) were accumulated based on the timestamp into a consistent database with the weather station parameters, T, RH, and effective wind.

### Chloride Deposition

Bi-weekly measurements of chloride deposition via wet candle chloride devices<sup>21</sup> were conducted over the year of 2021. Wet candle devices were deployed near Daytona Beach, FL at both IC and OS sites, as reported in prior work<sup>11,27</sup>. Chloride deposition at El Segundo and Whidbey Island were estimated based on a scaling factor. Specifically, contaminants measurements at all four locations were used to calculate scaling factors with Daytona Beach OS acting as the baseline measurement. It was assumed that the contaminants measurements (that is, electrolyte conductance) was linearly related to the chloride salt deposition density. Therefore, the scaling factors could be leveraged to estimate the salt deposition at all locations (Table 2).

**Table 1: Time range of data accumulation from three sources**

Measurement	Location	Start Date	End Date
<b><i>Sensing Devices</i></b>			
	<i>Daytona Beach OS</i>	12/21/2021	12/13/2022
	<i>Daytona Beach IC</i>	12/21/2021	12/13/2022
	<i>El Segundo</i>	1/11/2022	11/20/2022
	<i>Whidbey</i>	4/29/2022	4/21/2023
<b><i>1008 Witness Coupons</i></b>			
	<i>Daytona Beach OS</i>	12/21/2021	4/5; 6/21; 9/21; 12/22
	<i>Daytona Beach IC</i>	12/21/2021	4/5; 6/21; 9/21; 12/22
<b><i>NOAA Weather and Buoy Station</i></b>			
	<i>Daytona Beach</i>	12/20/2021	12/27/2022
	<i>El Segundo</i>	12/20/2021	12/27/2022
	<i>Whidbey</i>	4/29/2022	4/26/2023

### **Machine Learning Development**

Random Forest (RF) regression models were developed in python and R, with varying input features to predict the AA7075 free corrosion rate. Note that prior work in literature determined RF models to be the least sensitive to small training datasets<sup>10</sup>. If larger datasets were available, neural network models could be performed. The output goal of each model was to predict the corrosion, as measured by the real-time monitoring devices. A datasheet was accumulated with all possible features from the monitoring devices and NOAA data, as well as the target feature of corrosion, with aligned time-stamps to maintain consistency between daily cycles and yearly seasons. A 75/25 train/test split of the dataset was leveraged, independent of time. Train/test values were plotted, to ensure an even distribution of parameters, to mitigate any skewing. RF parameters were optimized for each model, including the number of trees and mtry parameters. Error metrics of R<sup>2</sup> were calculated on the 25% of testing data and are reported.

## **RESULTS**

### **Verification of Monitoring Device Measurements**

### Corrosion Rate Comparison with Witness Coupons

Although the 1008 carbon steel witness coupons represented corrosion of a different material than the sensing devices, the results could be qualitatively compared to confirm the relative severity of the OS and IC environments at Daytona Beach (Figure 3). The total accumulated charge measurement from the free corrosion sensor (that is, the proxy of self-corrosion of AA7075) tracked well through the year exposure with the mass-loss witness coupons, highlighting the validity of this approach. In addition, both samples and measurement techniques agreed in rank ordering of the environmental severities of the two Daytona Beach sites, indicating that the OS location resulted in higher corrosion rates.

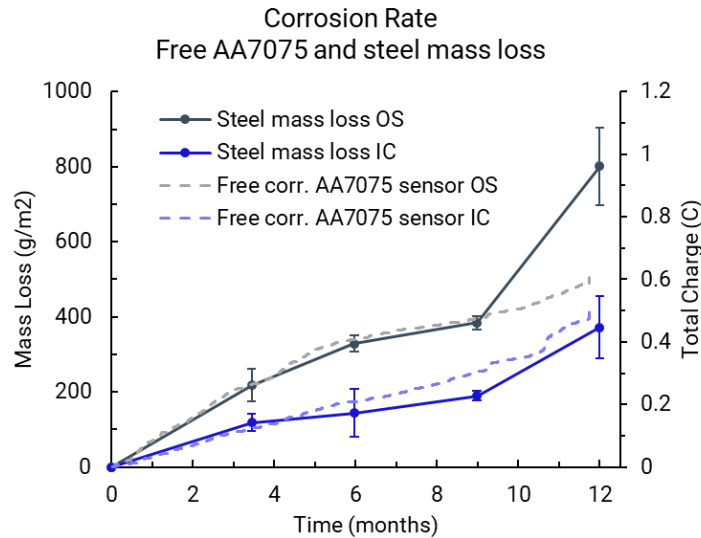
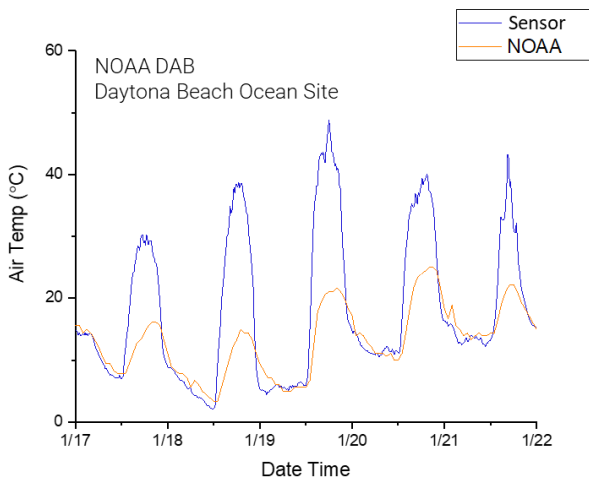


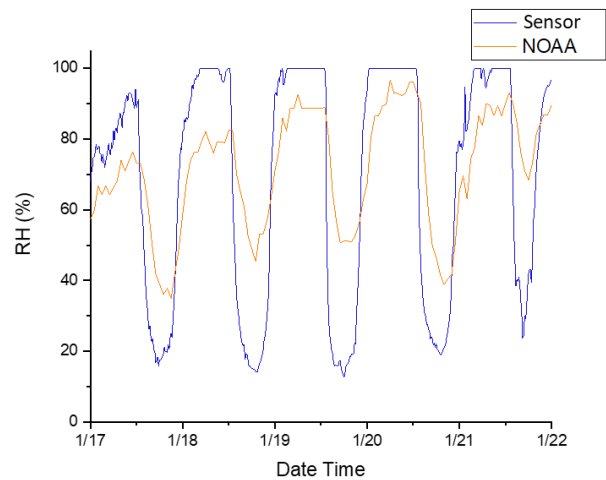
**Figure 3: Carbon steel (1008) mass loss overlaid with co-located real-time monitoring device measurements of accumulated charge at two adjacent Florida locations; near to the ocean (OS) and intracoastal (IC).**

### Environment Comparison with NOAA Measurements

The real-time environmental device measurements consisted of RH, T, and conductance. The diurnal cycle of the first two parameters could be compared directly with NOAA weather station measurements (Figure 4). Initial comparisons indicated the resolution of the real-time monitoring device to track diurnal cycles consistent with the NOAA measurements. The air temperature and RH are indirectly related; during the day, air temperature is at its peak and RH at its lowest point, while cooling during the evening results in the opposite effect<sup>22</sup>. Differences in the magnitudes of the air temperature and RH can directly be attributed to the monitoring device measurements being influence by solar irradiance heating and black body radiation cooling that do not affect the NOAA weather stations data; therefore, higher temperatures and lower RH is expected on the sensing devices during the day and higher RH at night.



(a)



(b)

**Figure 4: Comparison of real-time environment monitoring device and NOAA measurements of (a) air temperature and (b) RH at Daytona Beach, FL.**

As the conductance from the real-time monitoring devices represents a salt contaminant measurement, it could be compared directly with wet candle chloride measurements. In addition, the effective wind velocity and wave height are known to be contributors to salt deposition<sup>21</sup>; therefore, an accumulated metric of both parameters should also track with accumulation of salt contaminants. Note that wave, wind, and wet candle chloride measurements all assume a *total contaminant exposure*, neglecting wash/rain events that would remove salt from the surface. In contrast, the conductance measurement is real-time and takes into account wash/rain events.

The salt deposition from the accumulated wave and wind measurements were plotted alongside the OS, due to its closer proximity to the ocean (Figure 5). Relating accumulated wave and wind measurements to the IC site would then be scaled based on a “distance to seacoast” metric.

All OS salt accumulation metrics (wave, wind, wet candle, and conductance) tracked with each other very well over the year exposure (Figure 5). In particular, there was an increase in salt loading around April 29<sup>th</sup> 2022 that was captured through the wind, wet candle, and conductance. The wet candle and conductance measurements also both indicated that there was a larger accumulation of salt at the OS than IC site, which is consistent with literature that has documented a decay in corrosion as a function of the distance to the coast<sup>28</sup>.

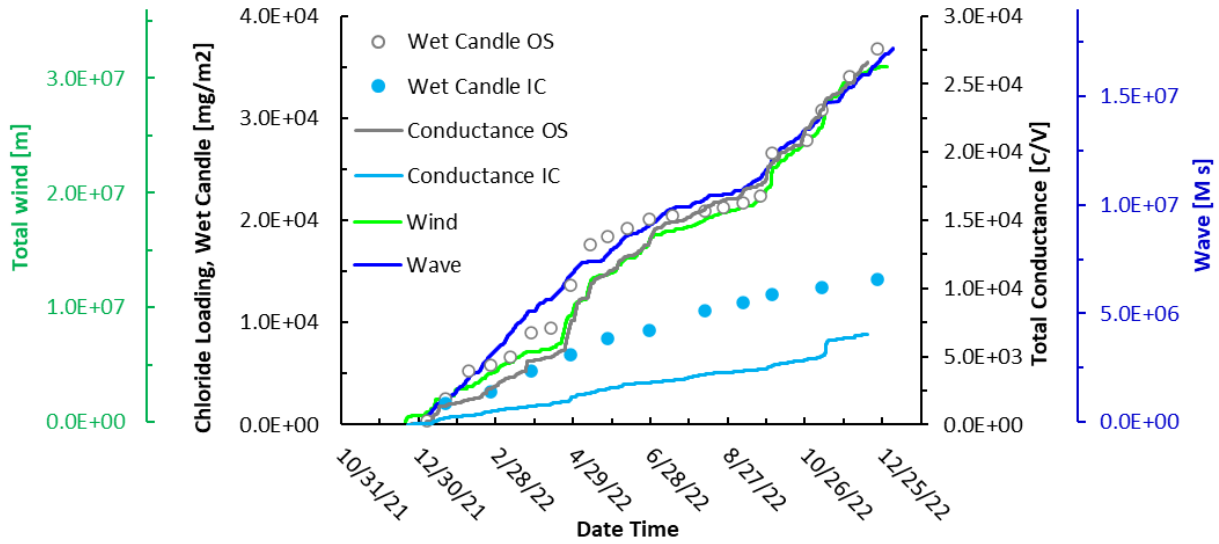


**Figure 5: Comparison of real-time monitoring device measurements (conductance) with NOAA weather (wind and wave) and wet candle chloride measurements at Daytona Beach, FL.**

Note that the maximum salt deposition through high effective wind and wave measurements do not necessarily align in timestamps with the maximum corrosion rate (Figure 6(a)). That is, although the wind and wave are contributing to salt deposition throughout the day, the corrosion generally only occurs at night in which there exists high RH and low T, allowing deliquescence to produce an electrolyte over the surface. Under those conditions, the high salt deposition during the day may still produce high corrosion rates at night, with some hours offset. This offset is in contrast to conductance, which also requires an electrolyte present for the measurement to be made, thereby resulting in strong alignment of peak values with the corrosion rate (Figure 6(b)). For rapid comparison of the offset, the year-exposure datasets were averaged based on hour and location to visualize hourly diurnal trends through all exposed days.

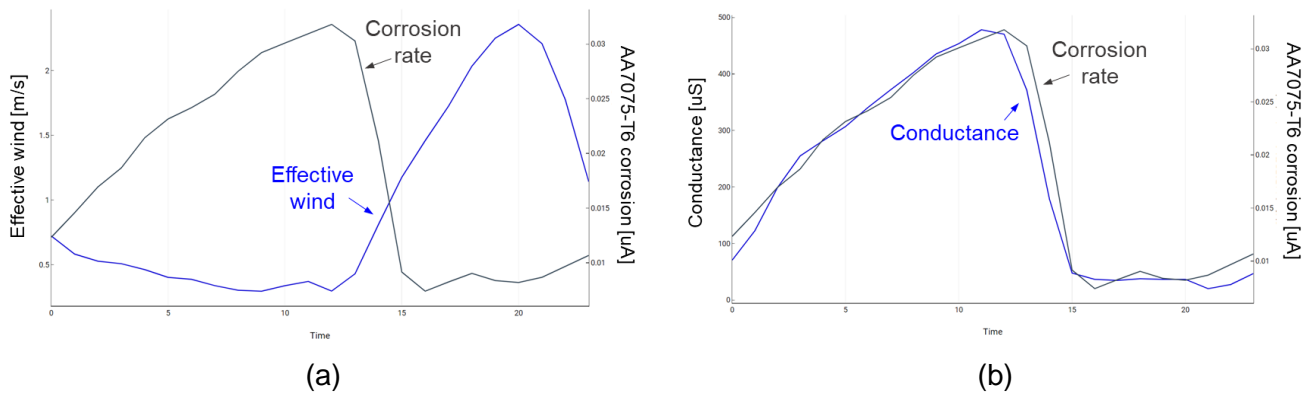


**Figure 6: Averaged daily hours at IC of (a) effective wind and (b) conductance, with free corrosion.**

To account for this offset, autocorrelations were conducted to relate wind and wave with conductance, respectively. A shift in the average daily hours over the year exposure resulted in good correlation between both metrics, with an example of OS indicated in Figure 7. The optimized shift in effective wind

with conductance was applied to the wave height, to maintain consistency in timestamps between the wind and wave parameters. This process was followed for each specific location prior to merging the datasets. A detailed analysis revealed that for a given location, the optimized shifting offset depended on the season, and corresponding month of the year. Offsets applied to the entire year of data lost this resolution. The autocorrelation and optimized shifting was automated to occur prior to any modeling of the data, and was applied to the hourly data.

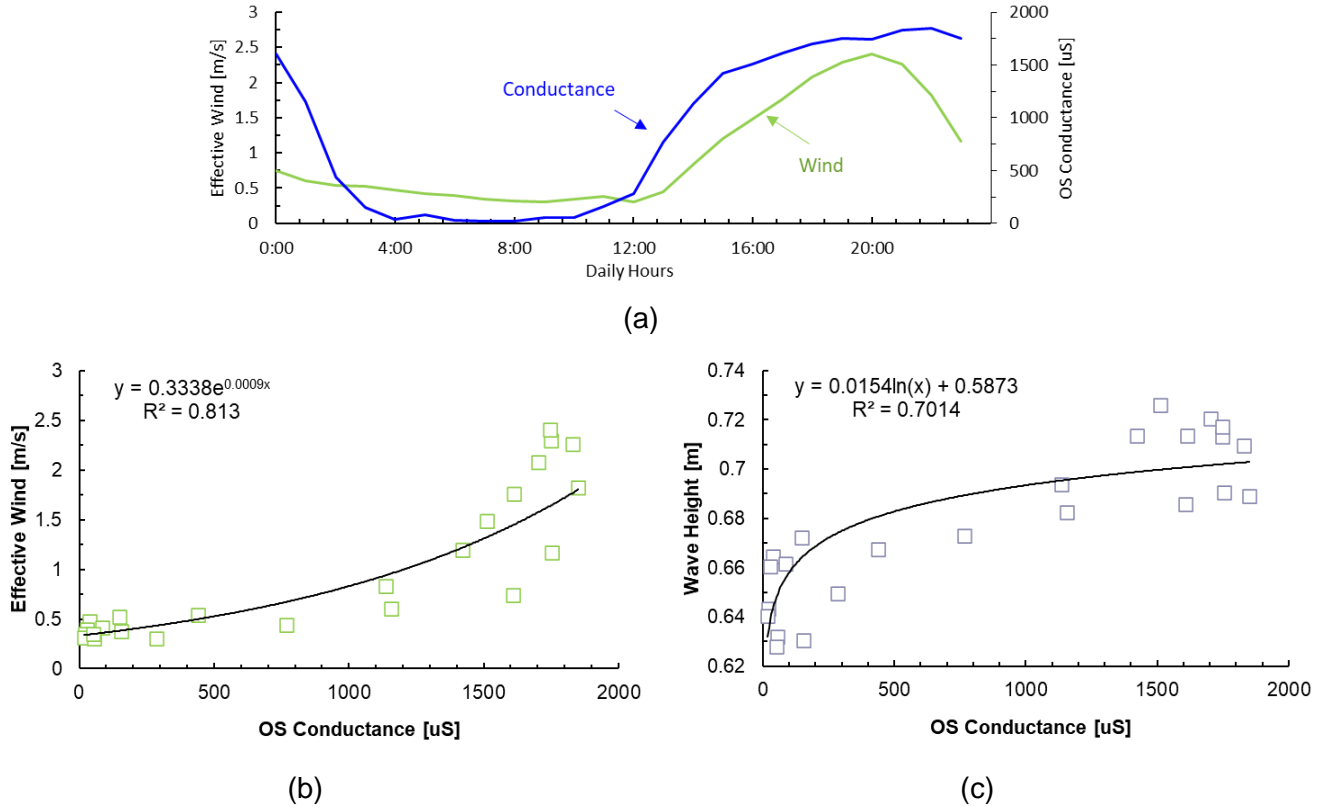


**Figure 7: (a) 10-hour lagged NOAA wind to correlate with OS monitoring device conductance over averaged daily hours, and (b) correlations with effective wind after shifting; (c) correlations with wave height after shifting.**

A summary of the annual averaged environmental metrics determined through NOAA, wet candle, and the sensing device was accumulated (Table 2). Although the annual averages provide a condensed table to be easily compared between the different data sources and locations, detailed real-time data with consistent time stamps was accumulated to be used as input features for the model.

**Table 2: Annual average data accumulation from three data sources for all locations of interest**

Location	NOAA				Monitoring Device			Wet Candle
	Avg. RH (%)	Avg. T (°C)	Eff. Wind (m)	Wave Height (M-s)	Avg. RH (%)	Avg. T (°C)	Cond. (C/V/a)	Annual Cl <sup>-</sup> dep. (mg/m <sup>2</sup> ·d)
<b>Daytona Beach (OS), FL</b>	74.8	22.4	31614	0.713	75.2	26.0	24228	108.4

<b>Daytona Beach (IC), FL</b>	74.8	22.4	31614	0.713	73.7	27.0	5577	43.8
<b>El Segundo, CA</b>	66.7	17.7	59874	1.004	65.5	23.8	45362	207.1*
<b>Whidbey Island, WA</b>	89.9	9.4	53414	0.395	79.7	12.5	19136	87.4*

*\*Estimated values*

## Machine Learning Models

After accumulating the environmental and corrosion database at the four locations of interest, four ML models were developed based on a tiered approach of input features ranging from less granular to more local and detailed, as summarized in Table 3. Initially, entire datasets of hourly measurements were applied, with a total of 35,119 observations. It was determined that the noise throughout the year was contributing to poor model performance. Therefore, two optimizations were conducted: 1) features were smoothed at a 3 to 4 hour resolution moving average, and 2) a single month of data was selected. The moving average was plotted against the raw data to confirm that the resolution of the parameters was not being removed. A single month was chosen to optimize the autocorrelation with wind and conductance.

Note that throughout all models, three main trends of the feature inputs followed: a temperature parameter, a RH parameter, and a salt accumulation parameter. Although RH is calculated through the temperature and absolute humidity, it provides valuable information on the formation of the electrolyte that is not present through temperature alone. Initial models with input parameters of either RH or temperature alone resulted in poor performance. During future development, these parameters could be accumulated into a single new parameter. In addition, the time of wetness, taking into account the time and duration of exposure to RH, has been found to be valuable and will be incorporated in future modeling efforts.

### 1<sup>st</sup> ML Model: Static Salt Assumption

The first model was trained on data with a static salt assumption for each location, based on the wet candle measurements from Daytona Beach. A static salt model is a close approximation of the environmental severity prescribed by ISO 9223, which uses yearly averages of environmental parameters such as a time of wetness (ToW), and chloride and sulfur dioxide deposition rates. A distance to seacoast metric was used to account for the differences between OS and IC Daytona Beach sites. All temperature and RH values were from the NOAA weather stations, representing the general environment without local measurements. Despite these features, the model performed poorly and was not able to accurately capture the corrosion rate (Table 3).

### 2<sup>nd</sup> ML Model: Dynamic Salt through Wind and Wave Data

To build on the prior model, dynamic salt accumulation was taken into account through the effective wind and wave measurements. The shifted wind and wave parameters were leveraged, to account for the early salt deposition. The temperature and RH parameters again were from the NOAA weather stations. Corrosion predictions largely increased in performance when leveraging a dynamic salt parameter, highlighting influence of capturing real-time salt deposition in contrast to annual averages (Table 3).

### 3<sup>rd</sup> ML Model: Local Salt Accumulation

Building again on the prior model, dynamic salt accumulation from the more local measurement of the monitoring device was taken into account. Specifically, the local conductance measurement at all

locations was leveraged, eliminating the need for a distance to seacoast feature. In addition, the conductance was seen to track well with the corrosion rate as a function of time, and therefore required no autocorrelation or offset was required (Figure 6b). The temperature and RH parameters were from the NOAA weather stations, consistent with the first two models. The performance of the model decreased slightly when incorporating this feature with NOAA RH and T (Table 3).

#### 4<sup>th</sup> ML Model: Local Environment Measurements

The last model leveraged all of the monitoring device measurements for the most local environment. As seen previously in Figure 4, the sensing device measurements track well with the diurnal cycle as measured by NOAA, with different maxima/minima that may be more relevant to actual structural materials. Incorporating these features with the conductance measurements resulted in the best performing model (Table 3 and Figure 8). Integrating the predicted corrosion rates, the total cumulative corrosion could be compared (Figure 9). The model predictions slightly underestimate the actual values, with a 5.2% error of the final cumulative value.

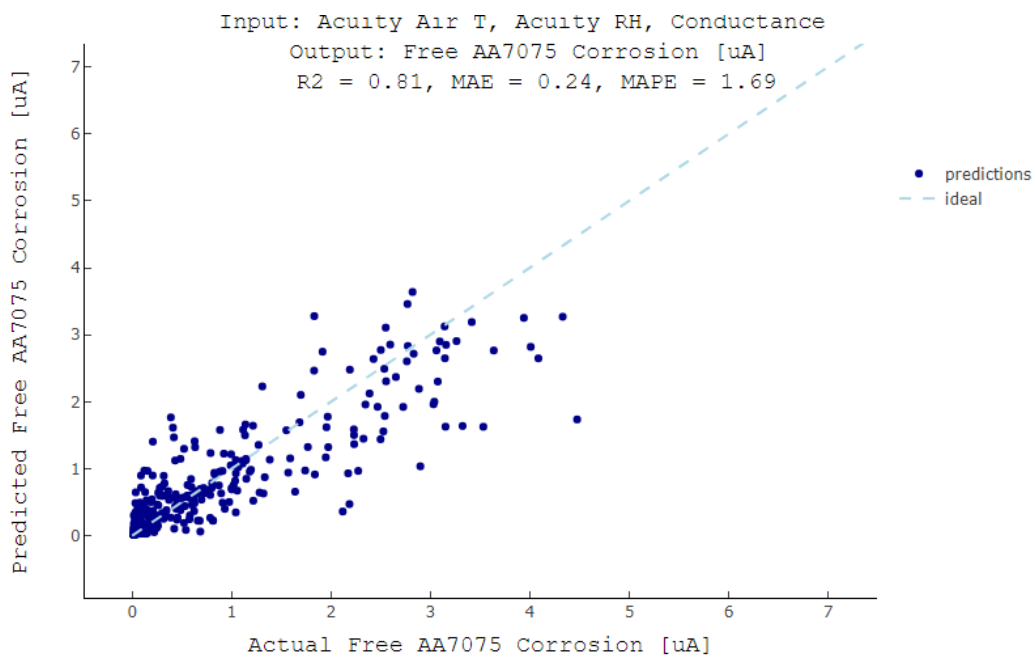


**Figure 8: Fourth ML prediction of corrosion rate as a function of measured (actual) corrosion rate, leveraging the Acuity RH, T, and conductance as input parameters.**

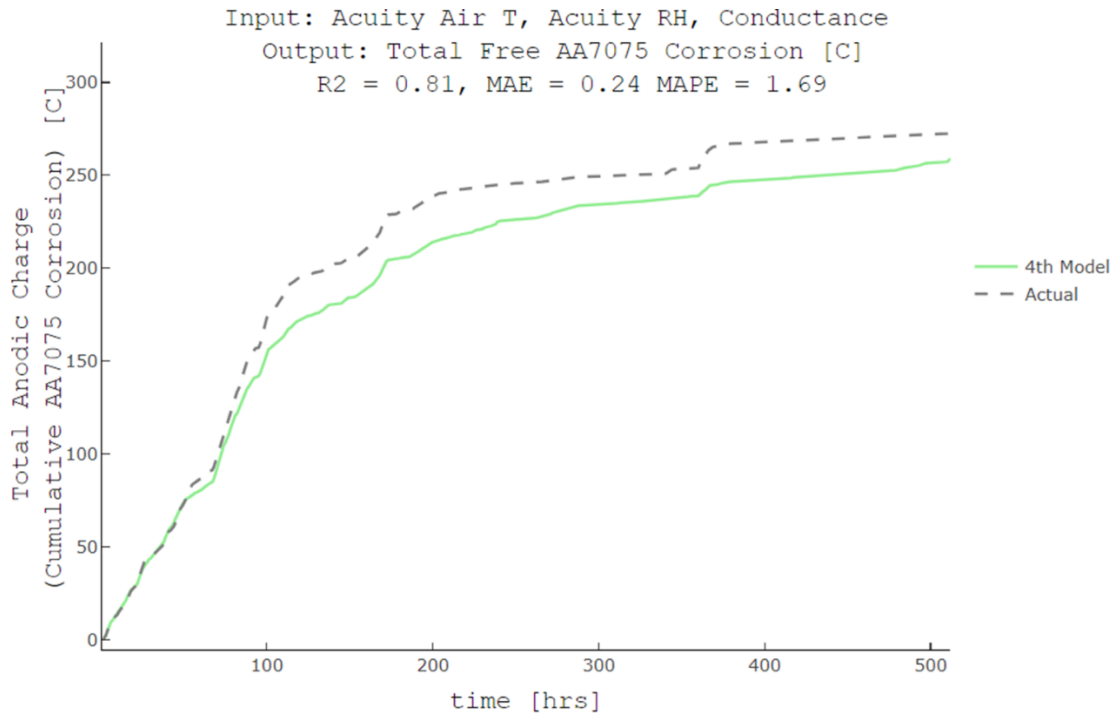


**Figure 9: Cumulative corrosion comparison with actual and predicted, as through the fourth ML model, leveraging the Acuity RH, T, and conductance as input parameters.**

**Table 3: Overview of four models developed in this work, leveraging data in month of November.**

Model #	Input Features									Testing Error
	NOAA				Monitoring Device			Wet Candle		R <sup>2</sup>
	RH (%)	T (°C)	Eff. Wind (m)	Wave Height (M-s)	RH (%)	T (°C)	Cond. (C/V/a)	Annual Cl-dep. (mg/m <sup>2</sup> -d)	Distance to coast [m]	Pred. Corrosion
1	X	X						X	X	0.64
2	X	X	X	X					X	0.72
3	X	X					X			0.68
4					X	X	X			0.81

## DISCUSSION

### Corrosion Prediction to Enhance Local Component Maintenance

Based on the tiered input features investigated, the best performing models occurred when dynamic salt accumulation or local environment measurements were incorporated. This result highlights the value of using dynamic and local environments in computational tools, as could be measured via facility/on-asset monitoring devices, rather than relying directly on annual averages. In addition, the good performance of the 2<sup>nd</sup> model highlights that NOAA effective wind and buoy wave height provide a good representation of dynamic salt accumulation, when local measurement devices are not available.

Once a model is optimized and trained on the features above, it can be used in tandem with corrosion maintenance manhour (MMH) models to help enhance long-term maintenance planning (Figure 10). In particular, environmental parameters influence the corrosion rate and resulting corrosion-related MMH; understanding these relationships can lead to forecasted severity and corrosion-related MMH for a given asset, thereby enabling informed maintenance scheduled intervals to enhance cost savings and asset availability.

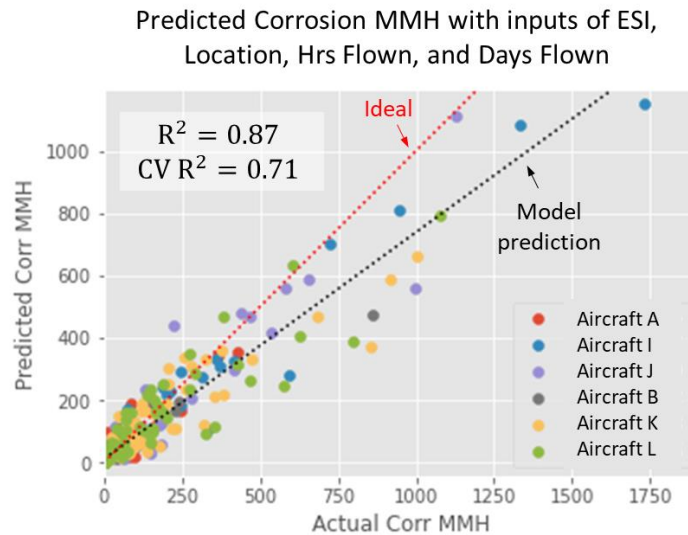


**Figure 10: ML prediction of corrosion maintenance manhours (MMH) of various aircraft, through input features of environmental severity index (ESI), aircraft location, hours flown, and days flown.**

### CONCLUSIONS

- Real-time monitoring devices and NOAA measurements were leveraged to train and test machine learning models to predict corrosion rate
- A tiered model approach was developed to determine the relative feature importance of specific environmental parameters
- Local environment measurements provided the best model approximation, in contrast to static annual average values
- Effective wind and wave height, scaled by a distance-to-seacoast factor, were determined to represent the delivery mechanisms of salt deposits and accumulation, thereby increasing model performance when local measurements are not available

### ACKNOWLEDGEMENTS

This material is based upon work supported by the Naval Air Warfare Center under Contract No. (N68335-22-C-0833) and the Office of Naval Research under Boeing prime ONR contract No. (N00014-20-C-1092). Any opinions, findings and conclusions or recommendations expressed in this material are those of the author(s) and do not necessarily reflect the views of NAVAIR or the Office of Naval Research.

## REFERENCES

1. Herzberg, E.F., S. Guo, A. Lai, and C.J. Marquardt, "The Annual Cost of Corrosion for the Facilities and Infrastructure of the Department of Defense Update" (2019).
2. Nickerson, W.C., M. Amiri, and N. Iyyer, *Corrosion Reviews* (2019).
3. Yoon, Y., J.D. Angel, and D.C. Hansen, *Corrosion* 72 (2016): pp. 1424–1432.
4. Sanders, C.E., and R.J. Santucci, *Corrosion and Materials Degradation* 4 (2022): pp. 1–17.
5. Dean, S.W., Dagmar. Knotkova, Katerina. Kreislova, ASTM Committee G-1 on Corrosion of Metals., ASTM International., and ISOCORRAG International Atmospheric Exposure Program., *ISOCORRAG International Atmospheric Exposure Program : Summary of Results* (n.d.).
6. Kopitzke, S., "Characterizing Environmental Severity for Naval Air Stations" (n.d.).
7. "ISO 9223 Corrosion of Metals and Alloys - Corrosivity of Atmospheres - Classification, Determination and Estimation," Reference number ISO (2012).
8. "ISO 9224 Corrosion of Metals and Alloys - Corrosivity of Atmospheres - Guiding Values for the Corrosivity Categories," Reference number ISO (2012).
9. Silver, N.A., and W. Gaebel, "Facilities Environmental Severity Classification Study Final Report" (2017), [www.corrdefense.org](http://www.corrdefense.org).
10. Coelho, L.B., D. Zhang, Y. Van Ingelgem, D. Steckelmacher, A. Nowé, and H. Terryn, "Reviewing Machine Learning of Corrosion Prediction in a Data-Oriented Perspective," *npj Materials Degradation* (Nature Publishing Group, 2022).
11. Agnew, L., V. Avance, B. Clark, and F. Friedersdorf, "Atmospheric Environment Severity Monitoring for Corrosion Management," in AMPP (Denver, CO, 2023).
12. Marshall, R.S., R. Kelly, A. Goff, and C. Sprinkle, *Corrosion* 75 (2019): pp. 1461–1473.
13. Marshall, R., K.A. Define, R.S. Rosner, A. Goff, C. Sprinkle, P.V. Balachandran, and R.G. Kelly, *Corrosion* 79 (2023).
14. Snihirova, D., D. Höche, S. Lamaka, Z. Mir, T. Hack, and M.L. Zheludkevich, *Corros Sci* 157 (2019): pp. 70–78, <https://doi.org/10.1016/j.corsci.2019.04.036>.
15. Williams, K.S., and R.J. Thompson, *Corrosion* 75 (2019): pp. 474–483.
16. Taylor, C.D., *Corrosion Engineering Science and Technology* 50 (2015): pp. 490–508.
17. Chen, Z.Y., D. Liang, G. Ma, G.S. Frankel, H.C. Allen, and R.G. Kelly, *Corrosion Engineering Science and Technology* 45 (2010): pp. 169–180.
18. Taylor, C.D., D. Borth, and D.C. Hansen, "Environmental Exposure Profiles for Atmospheric Corrosion" (2023).
19. Yoon, Y., J.D. Angel, and D.C. Hansen, *Corrosion* 72 (2016): pp. 1424–1432.
20. Cole, I.S., W.D. Ganther, J.D. Sinclair, D. Lau, and D.A. Paterson, *J Electrochem Soc* 151 (2004): p. B627.
21. Pham, N.D., Y. Kuriyama, N. Kasai, S. Okazaki, K. Suzuki, and D.T. Nguyen, *Atmos Environ* 198 (2019): pp. 46–54.
22. Schindelholz, E., R.G. Kelly, I.S. Cole, W.D. Ganther, and T.H. Muster, *Corros Sci* 67 (2013): pp. 233–241.
23. Pei, Z., D. Zhang, Y. Zhi, T. Yang, L. Jin, D. Fu, X. Cheng, H.A. Terryn, J.M.C. Mol, and X. Li, *Corros Sci* 170 (2020).

24. Yan, L., Y. Diao, Z. Lang, and K. Gao, *Sci Technol Adv Mater* 21 (2020): pp. 359–370.
25. Clark, B., J. Wright, F. Friedersdorf, R. Meekins, and L. Agnew, “Measurement and Prediction of Aerospace Corrosion Rate Using Real-Time Sensor Measurements and Machine Learning Approaches,” in *CORROSION 2020*, Paper No. NACE-2020-14884 (2020).
26. Spooner, M., R. Ambat, H. Conseil-Gudla, and M. Kulahci, *Machine Learning with Applications* 9 (2022): p. 100397, <https://linkinghub.elsevier.com/retrieve/pii/S2666827022000767>.
27. Friedersdorf, F., and L. Agnew, “Use of Environment and Corrosivity Monitoring to Characterize Base and Airframe Severity,” in *NATO STO-MP-AVT-373* (Sweden, 2023).
28. Cole, I., P. Corrigan, and N.V. Hue, *CORROSION SCIENCE AND TECHNOLOGY* 11 (2012): pp. 103–107.